

Helical textures in $^3\text{He-A}$ and magnetic resonance

Y. R. Lin-Liu, Dieter Vollhardt, and Kazumi Maki

Department of Physics, University of Southern California,

Los Angeles, California 90007

(Received 8 December 1978)

The existence of helical textures in $^3\text{He-A}$ in the presence of both superflow and magnetic field is established theoretically. The magnetic resonance frequencies of the helical textures are determined.

I. INTRODUCTION

Superflow in $^3\text{He-A}$ is one of the most fascinating subjects of superfluid ^3He . Making use of an elegant topological argument, Volovik and Mineyev¹ have shown that a $^3\text{He-A}$ state with superflow in a torus is globally unstable. It has been conjectured that such an instability may be catalysed by coreless vortices²⁻⁴ for example. Recently, on the other hand, Bhattacharyya *et al.*⁵ have shown that a uniform texture with $\hat{l} \parallel \hat{d} \parallel \vec{v}_s$ is locally stable in the dipole-locked limit and in the vicinity of the transition temperature T_c , but becomes unstable at T_i , where

$$\kappa [\equiv K_b \rho_0 (\frac{1}{2} \rho_s^{\parallel} + c_0)^{-2}] = 1 .$$

Here \hat{l} and \hat{d} are the orbital vector and spin vector describing the condensate of $^3\text{He-A}$ and K_b , ρ_0 , etc., are coefficients of the texture free energy.^{2,6} It has been later shown^{7,8} that below T_i there is a class of helical textures, where both \hat{l} and \hat{d} wind around \vec{v}_s , which are locally stable. It is of some interest to point out that the nuclear dipole energy plays a crucial role in the stability of the helical texture as well as that of the parallel texture⁵ ($\hat{l} \parallel \hat{d} \parallel \vec{v}_s$). For example, in the dipole free case none of these textures are locally stable in the presence of superflow. More recently we have shown⁹ that the helical texture can be stabilized even in the vicinity of the transition temperature (i.e., the Ginzburg-Landau regime) by applying a magnetic field. In fact a similar idea has been conceived by several authors¹⁰ independently, although all of them considered the dipole-locked case only. As we shall see later, this assumption is only valid in the limit of small superflow and magnetic field.

The object of the present paper is to study the helical texture both in superflow and a magnetic field.⁹ In this case \hat{d} is no longer necessarily parallel to \hat{l} .

For simplicity we limit ourselves to the cases $\vec{v}_s \parallel \vec{H}$ and $\vec{v}_s \perp \vec{H}$ and the Ginzburg-Landau regime, where \vec{H} is the magnetic field vector. The effects of a small tilt of the magnetic field are considered in Appendix A. It is shown that in the presence of a magnetic field the helical texture is stable in an extended region in the v_s - H phase diagram even in the Ginzburg-Landau regime.

A large portion of this paper is devoted to the calculation of the nuclear-magnetic-resonance (NMR) frequencies. In the case of the parallel geometry ($\vec{v}_s \parallel \vec{H}$), the helical texture possesses two distinct longitudinal resonance frequencies and four distinct transverse resonance frequencies. Furthermore, both of the transverse frequencies do not satisfy the Pythagorean rule¹¹; the magnetic field induces a more complicated field dependence. In the perpendicular geometry ($\vec{v}_s \perp \vec{H}$), on the other hand, the longitudinal and the transverse resonance frequencies are given by

$$\omega_l^2 = \omega_0^2 + \lambda_l \Omega_A^2 ,$$

$$\omega_t^2 = \omega_0^2 + \lambda_t \Omega_A^2 ,$$

where ω_0 is the Larmor frequency, Ω_A is the Leggett frequency in $^3\text{He-A}$, and λ_l and λ_t are constants depending on H and are much larger than unity. The explicit values of λ_l and λ_t are calculated numerically. We believe that the NMR will provide an unambiguous test for the existence of the helical texture.

In the course of the present work we have learned of experimental work by Kleinberg¹² at La Jolla, who measured zero sound attenuation perpendicular to the heat current in the presence of a magnetic field parallel to the heat current. His low heat current data ($J_h \sim 1$ n watt/cm²) appear to be consistent with the existence of the helical texture predicted here, although certainly more work has to be done before we draw a definite conclusion.

II. HELICAL TEXTURES

We will consider two configurations, where the magnetic field is either parallel or perpendicular to the superflow. Furthermore, we limit ourselves to the case where the textures depend only on z , the direction of the superflow. Indeed, in the limit of small deviations of \hat{l} and \hat{d} from the z direction the

transverse fluctuation with $\vec{k} \perp \vec{v}_s$ is not important (see Appendix B).

A. $\vec{H} \parallel \vec{v}_s$

In reduced units the free-energy in the presence of superflow and an external magnetic field is given by¹³

$$G = -(1+s)^{-1}p^2 + \frac{1}{2}(3-2s)\chi_z^2 + (1+s)\theta_z^2 + \frac{2(1-s)^{1/2}}{(1+s)}p\psi_z + s\left(\frac{2}{1+s} - \frac{1}{2}\right)\psi_z^2 + \sin^2\theta(1+s)\phi_z^2 + \{1 - [\cos\chi\cos\theta + \sin\chi\sin\theta\cos(\psi-\phi)]^2\} + h^2\cos^2\theta, \quad (1)$$

where

$$s = \sin^2\chi, \quad p = \frac{(1+s)v_s}{v_{s0}}, \quad h = \frac{H}{H_0},$$

$$v_{s0} = \frac{\hbar}{2m} \left[\frac{\chi_N \Omega_A^2(T)}{\rho_{s\parallel}(T)} \right]^{1/2} = \frac{\hbar}{(2)^{1/2} m \xi_L} \simeq 0.1 \text{ cm/sec},$$

$$H_0 = \Omega_A(T) \left[\frac{\chi_N}{\Delta\chi} \right]^{1/2} \sim 20 \text{ Oe},$$

and p is the normalized mass current, H is the external magnetic field ($\parallel \vec{v}_s$), ξ_L is the dipolar coherence length ($\sim 10 \mu$), and $\Delta\chi$ is the anisotropic part of the

magnetic susceptibility. Here we have parametrized \hat{l} and \hat{d} as

$$\hat{l} = (\sin\chi\cos\psi, \sin\chi\sin\psi, \cos\chi), \quad (2)$$

$$\hat{d} = (\sin\theta\cos\phi, \sin\theta\sin\phi, \cos\theta).$$

To study the stability of the uniform texture ($\hat{l} \parallel \hat{d} \parallel \vec{v}_s$) and helical textures with small inclinations χ and θ , it is more convenient to introduce new parameters $u, v, u',$ and v' ;

$$u = \sin\chi\cos\psi, \quad v = \sin\chi\sin\psi, \quad (3)$$

$$u' = \sin\theta\cos\phi, \quad v' = \sin\theta\sin\phi.$$

Then the free-energy G is rewritten

$$G = G_0 + G_1 + G_2,$$

$$G_0 = -p^2 + 2p\psi_z,$$

$$G_1 = \frac{3}{2}(u_z^2 + v_z^2) - 3p(uv_z - vu_z) + (u_z'^2 + v_z'^2) + p^2(u^2 + v^2) - h^2(u'^2 + v'^2) + (u - u')^2 + (v - v')^2, \quad (4)$$

$$G_2 = (u^2 + v^2) \left[\frac{1}{2}(u_z^2 + v_z^2) + \frac{11}{4}p(uv_z - vu_z) + (u_z'^2 + v_z'^2) - p^2(u^2 + v^2) \right] + (u'u_z' + v'v_z')^2 - \frac{5}{2}(uv_z - vu_z)^2 + [u(u - u') + v(v - v')] \cdot [u'(u - u') + v'(v - v')],$$

where we have kept up to quartic terms in u, v , etc.

We have here a Ginzburg-Landau-type functional with the four component field (u, v, u', v') . The quadratic term is minimized by choosing

$$u = u_0 \cos(kz), \quad v = u_0 \sin(kz), \quad (5)$$

$$u' = u_0' \cos(kz), \quad v' = u_0' \sin(kz),$$

where k is measured in units of $(2)^{1/2}\xi_L^{-1}$. By minimizing $\langle G_1 \rangle$, the space average of G_1 in terms of u_0' , we obtain

$$u_0' = (1 - h^2 + k^2)^{-1} u_0. \quad (6)$$

The inclination of \hat{d} is different from that of \hat{l} except when $h^2 - k^2 = 0$.

Substituting u_0' thus determined into G and taking the space average, we have

$$\langle G \rangle = \langle G_0 \rangle + A(k)u_0^2 + \frac{1}{2}B(k)u_0^4, \quad (7)$$

where

$$A(k) = p^2 + \frac{3}{2}k^2 - 3pk + 1 - (1 - h^2 + k^2)^{-1},$$

$$B(k) = 2(h^2 - k^2)^2(1 - h^2 + k^2)^{-3} + 2k^2(1 - h^2 + k^2)^{-2} - 2p^2 - 4k^2 + \frac{11}{2}pk. \quad (8)$$

From the free-energy (7), we conclude that (i) when

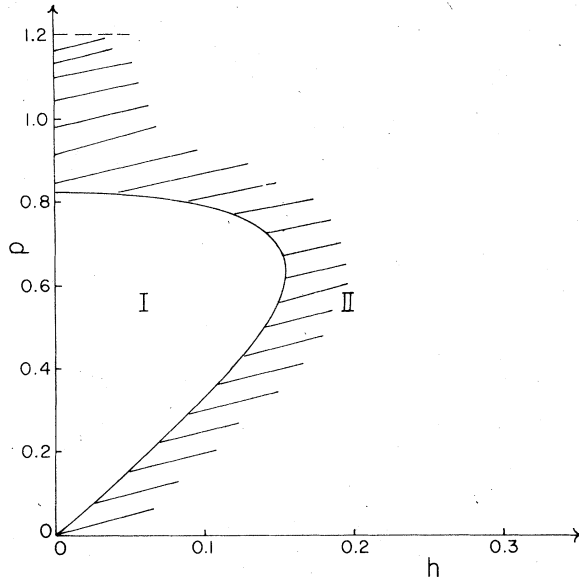


FIG. 1. Phase diagram for $\vec{v}_s \parallel \vec{H}$. In region I the uniform texture ($\hat{l} \parallel \hat{d} \parallel \vec{v}_s$) is stable; it is surrounded by region II where the helical texture is stable. Above $p = 1.2$, the helical texture becomes locally unstable.

$A(k) > 0$ for all k , the uniform texture with $\hat{l} \parallel \hat{d} \parallel \vec{v}_s$ is locally stable. (ii) When $A(k) \geq A(k_m) = 0$ and the equality is satisfied by a single $k = k_m$, and furthermore, $B(k_m) > 0$, the uniform texture becomes unstable against the appearance of the helical texture with pitch $k = k_m$. Therefore this condition gives the phase boundary between the uniform texture and the helical texture. (iii) When $A(k_m) < 0$, and $B(k_m) > 0$, the helical texture with pitch $k = k_m$ and $u_0^2 = |A|/B$ is locally stable. (iv) When $A(k_m) < 0$, and $B(k_m) < 0$, the uniform texture as well as the helical texture are unstable.

From the above criteria, we have constructed the phase diagram shown in Fig. 1. In region I the uniform texture ($\hat{l} \parallel \hat{d} \parallel \vec{v}_s$) is locally stable. Region I is completely surrounded by region II (the shaded area), where the helical textures are stable. Near the origin ($p = h = 0$), the phase boundary is given by $p = (10)^{1/2} h$. This slope agrees with other calculations,¹⁰ where \hat{d} and \hat{l} are assumed to be dipole locked. In fact, near the origin \hat{d} and \hat{l} are parallel to each other as seen from Eq. (6). The stability region of the uniform texture terminates even in the absence of magnetic field at $p = 0.826$ contrary to the result of the dipole-locked calculation.¹⁰ In fact for $p > 0.826$; \hat{d} and \hat{l} are no longer parallel to each other. Furthermore, we find in the limit $h \rightarrow 0$, $B(k_m)$ becomes negative when $p > 1.20$. This implies that in the region $p > 1.20$ the helical textures are no

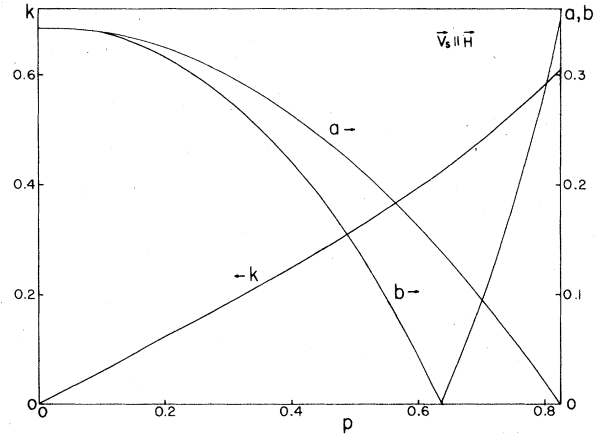


FIG. 2. Coefficients, a , b , and the pitch k of the helical texture at the phase boundary are shown as functions of p .

longer stable. However, whether this means the total collapse⁴ of a state with uniform flow is not clear.

In the vicinity of the phase boundary, where χ and θ are still small, we have

$$\sin^2 \chi = |u_0|^2 = a(h - h_l)/h_l, \quad \text{for } h > h_l, \quad (9)$$

where

$$a = h \left| \frac{\partial A}{\partial h} \right|_{h=h_l} B^{-1}$$

and $h_l = h_l(p)$ is the reduced magnetic field at the phase boundary. The pitch k as well as coefficients a and b ($\equiv p_l |(\partial A / \partial p)|_{p=p_l} B^{-1}$) are calculated numerically along the phase boundary and are shown in Fig. 2 as functions of p . In particular in the vicinity of the origin Eq. (9) reduces to

$$\sin^2 \chi = \frac{10}{29} \left(\frac{h - h_l}{h_l} \right)$$

B. $\vec{H} \perp \vec{v}_s$

In this case both magnetic field and superflow stabilize the parallel configuration ($\hat{l} \parallel \hat{d} \parallel \vec{v}_s$), although this uniform configuration decays into an elliptically polarized helical texture for $p \geq 0.826$.

The free-energy is still given by Eq. (1), except the last term $h^2 \cos^2 \theta$ has to be replaced by $h^2 \sin^2 \theta \sin^2 \phi$ (here we assumed that the magnetic field is along the y direction). Similarly in Eq. (3), the h -dependent term in G_1 has to be replaced by $h^2 (v')^2$. In the present case the magnetic field breaks the axial sym-

metry. The free-energy is minimized by choosing

$$u = u_0 \cos(kz), \quad v = v_0 \sin(kz),$$

$$u' = u_0' \cos(kz), \quad v = v_0' \sin(kz),$$

and

$$u_0' = (1 + k^2)^{-1} u_0, \quad v_0' = (1 + k^2 + h^2)^{-1} v_0, \quad (10)$$

and

$$(u_0/v_0)^2 = (K_2/K_1)^2,$$

where

$$K_1 = (p^2 + \frac{3}{2}k^2 + 1 - \delta_1)^{1/2},$$

$$K_2 = (p^2 + \frac{3}{2}k^2 + 1 - \delta_2)^{1/2},$$

$$\delta_1 = (1 + k^2)^{-1},$$

and

$$\delta_2 = (1 + k^2 + h^2)^{-1}. \quad (11)$$

Introducing a new variable by $\bar{u}_0 = (u_0 v_0)^{1/2}$, we have

$$\langle G \rangle = \langle G_0 \rangle + A(k) |\bar{u}_0|^2 + \frac{1}{2} B(k) |\bar{u}_0|^4, \quad (12)$$

$$A(k) = K_1 K_2 - 3pk,$$

$$B(k) = \frac{1}{4} \left[\left(\frac{K_2}{K_1} \right)^2 \left[3\delta_1(1 - \delta_1)^2 + \frac{1}{2}k^2(1 + 2\delta_1^2 + 2\delta_1^4) - 3p^2 \right] + \left(\frac{K_1}{K_2} \right)^2 \left[3\delta_2(1 - \delta_2)^2 + \frac{1}{2}k^2(1 + 2\delta_2^2 + 2\delta_2^4) - 3p^2 \right] - 17k^2 - 2p^2 + [3(\delta_1^2 + \delta_2^2) - 2\delta_1^2\delta_2^2]k^2 + (1 - \delta_1)(1 - \delta_2)(\delta_1 + \delta_2) \right] + \frac{11}{4}pk \left(\frac{K_2}{K_1} + \frac{K_1}{K_2} \right). \quad (13)$$

For the free-energy (12), we can apply the same criteria as formulated below Eq. (8). From this we have constructed the phase diagram, which is shown in Fig. 3. As expected, in the transverse geometry ($\vec{H} \perp \vec{v}_s$), the stability region I of the parallel texture ($\hat{l} \parallel \vec{d} \parallel \vec{v}_s$) is much more extended than in the case $\vec{H} \parallel \vec{v}_s$. In the figure we have inserted by a broken line the corresponding stability region in the case $\vec{H} \parallel \vec{v}_s$, for comparison. Furthermore, the stability region II of the helical texture appears to be bounded both in superflow and magnetic field. We have indicated this intrinsic instability region by a broken line

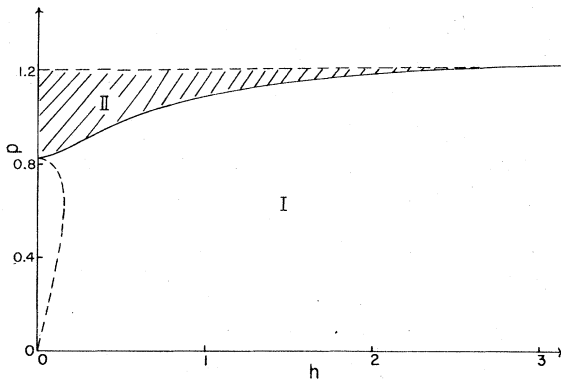


FIG. 3. Phase diagram for $\vec{v}_s \perp \vec{H}$. In region I the uniform texture ($\hat{l} \parallel \vec{d} \parallel \vec{v}_s$) is stable, while in region II the helical texture becomes stable. The stability region of the helical texture is again limited by $p \approx 1.2$.

connecting two points where $B(k_m) = 0$. Just above the region I, the inclination of the \hat{l} vector is given by

$$\begin{aligned} \sin^2 \chi &= |\bar{u}_0|^2 = a(h - h_l')/h_l' \\ &= b(p - p_l')/p_l', \end{aligned} \quad (14)$$

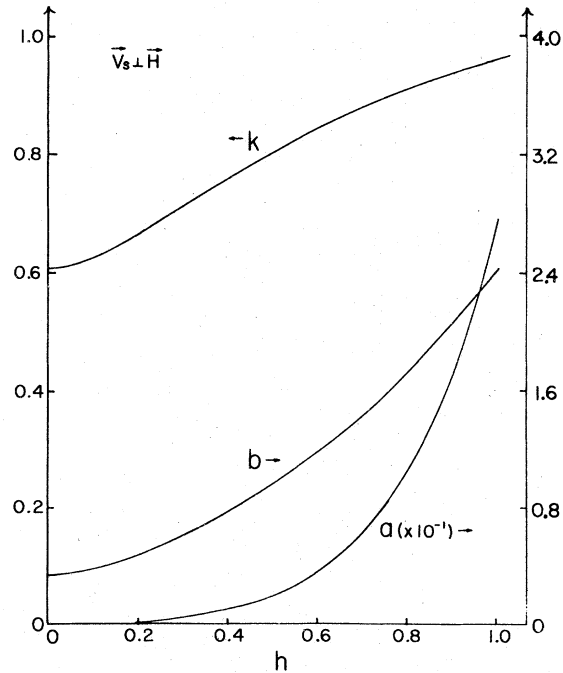


FIG. 4. Coefficients a , b , and the pitch k at the phase boundary are shown as functions of h .

where

$$a = h_l' \left| \frac{\partial A}{\partial h} \right|_{h=h_l'} B^{-1}$$

and

$$b = p_l' \left| \frac{\partial A}{\partial p} \right|_{p=p_l'} B^{-1}$$

and $h_l'(p)$ and $p_l'(h)$ are the field and the mass current at the phase boundary. The pitch k at the phase boundary as well as a and b are numerically evaluated and are shown in Fig. 4 as functions of h .

III. MAGNETIC RESONANCES

Although a sound propagation experiment senses the average orientation of the \hat{l} vector,¹² a nuclear-magnetic-resonance experiment appears to provide a far more sensitive probe to the helical texture.⁹ This is because the NMR frequencies reflect details of the \hat{d} and \hat{l} orientations and can be considered the unique signature of the underlying texture. We shall consider the NMR frequencies for two geometrical set ups separately.

A. $\vec{H} \parallel \vec{v}_s$

In this case the magnetic resonance in the parallel texture $\hat{l} \parallel \hat{d} \parallel \vec{v}_s$ is somewhat unusual, since the longitudinal rf field does not couple to the \hat{d} vector. Therefore, there is no longitudinal resonance although the transverse resonance takes place at¹⁴

$$\omega_t = \left[\frac{1}{4} \omega_0^2 + \Omega_A^2 \right]^{1/2} + \frac{1}{2} \omega_0,$$

where Ω_A is the Leggett frequency in $^3\text{He-A}$ and ω_0 is the Larmor frequency.

The magnetic resonance in the helical texture may be most conveniently formulated in terms of Euler angles (α, β, γ) . First of all the magnetization \vec{M} is related to the time derivative of Euler angles by¹⁵

$$\begin{aligned} \omega_1 &= \cos \alpha \sin \beta \gamma_t - \sin \alpha \beta_t, \\ \omega_2 &= \sin \alpha \sin \beta \gamma_t + \cos \alpha \beta_t, \\ \omega_3 &= \alpha_t + \cos \beta \gamma_t, \\ (\vec{M} &= -\gamma_0 \chi_N \vec{\omega}) \end{aligned} \quad (15)$$

Furthermore \hat{d} is given by

$$\hat{d} = (\sin \beta \cos \alpha, \sin \beta \sin \alpha, \cos \beta). \quad (16)$$

The Lagrangian describing the spin dynamics is given

by $L = T - V$, where

$$T = \frac{1}{2} \chi_N \int d^3r [\alpha_t^2 + \beta_t^2 + \gamma_t^2 + 2\alpha_t \gamma_t \cos \beta - 2\omega_0(\alpha_t + \gamma_t \cos \beta)]$$

and

$$V = \frac{1}{2} \chi_N \Omega_A^2 G. \quad (17)$$

Then the oscillation of \hat{d} around a helical texture is parametrized as

$$\begin{aligned} \hat{d} &= (\sin(\theta + g) \cos(\phi + f), \\ &\sin(\theta + g) \sin(\phi + f), \cos(\theta + g)), \end{aligned} \quad (18)$$

where now θ and $\phi (= kz)$ are those angles describing the helical texture and f and g describe small fluctuations. From the Lagrangian (17) we obtain the following linearized equations:

$$\begin{aligned} f_u + \gamma_u \cos \theta &= -\frac{1}{2} \Omega_A^2 \left(\frac{\delta G}{\delta f} \right), \\ g_u - \omega_0 \gamma_t \sin \theta &= -\frac{1}{2} \Omega_A^2 \left(\frac{\delta G}{\delta g} \right), \\ \gamma_u + f_u \cos \theta + \omega_0 g_t \sin \theta &= 0, \end{aligned} \quad (19)$$

where

$$\begin{aligned} \frac{1}{2} \frac{\delta G}{\delta f} &= -\sin^2 \theta (1+s) f_{zz} + \sin \theta \sin \chi \cos(\theta - \chi) f \\ &\quad - 2 \sin \theta \cos \theta (1+s) k g_z, \\ \frac{1}{2} \frac{\delta G}{\delta g} &= -(1+s) g_{zz} \\ &\quad + [k^2 \cos(2\theta) (1+s) + \cos(2(\theta - \chi))] g \\ &\quad + 2 \sin \theta \cos \theta (1+s) k f_z, \end{aligned} \quad (20)$$

and we have identified $\alpha = \phi + f$ and $\beta = \theta + g$. In the helical texture three variables (f, g, γ) are coupled to each other. However, the variable γ can be easily eliminated. Then a spin-wave solution of the form $f, g \propto \exp[i(qz - \omega t)]$ is determined by

$$\begin{aligned} (\omega^2 - L_{11} \Omega_A^2) \sin \theta f \\ - i(\omega \omega_0 - L_{12} \Omega_A^2) \cos \theta g &= 0, \\ (\omega^2 - \omega_0^2 \sin^2 \theta - L_{22} \Omega_A^2) g \\ + i(\omega \omega_0 - L_{12} \Omega_A^2) \sin \theta \cos \theta f &= 0, \end{aligned} \quad (21)$$

where

$$\begin{aligned} L_{11} &= \frac{\sin\chi \cos(\chi - \theta)}{\sin\theta} + (1+s)q^2, \\ L_{22} &= \left[\frac{\sin 2\chi}{\sin 2\theta} \right] - h^2 \cos 2\theta + (1+s)q^2, \\ L_{12} &= 2kq(1+s). \end{aligned} \quad (22)$$

The spin-wave dispersion is given by the roots of

$$(\omega^2 - L_{11}\Omega_A^2)(\omega^2 - \omega_0^2 \sin^2\theta - L_{22}\Omega_A^2) - (\omega\omega_0 - L_{12}\Omega_A^2)^2 \cos^2\theta = 0. \quad (23)$$

In the vicinity of the phase boundary where both χ and θ are small, the spin-wave dispersion is given by

$$\omega_{1,2}(q) = [(\lambda_l + q^2 \pm 2kq)\Omega_A^2 + \frac{1}{4}\omega_0^2]^{1/2} \pm \frac{1}{2}\omega_0, \quad (24)$$

where

$$\begin{aligned} \lambda_l &= \lim_{h \rightarrow h_1 + 0} \left[\frac{\sin\chi}{\sin\theta} \right] \\ &= (1 - h_1^2 + k^2). \end{aligned}$$

In deriving Eq. (24), we have neglected a term proportional to h^2 in L_{22} , which is always small at the phase boundary. The quantity λ_l is calculated numerically along the phase boundary and shown as a function of p in Fig. 5. λ_l increases monotonically from $\lambda_l = 1$ to $\lambda_l = 1.37$, as p increases from 0 to $p_c = 0.826$.

Within the above spin wave, the longitudinal rf field couples to the homogeneous mode (i.e., $q = 0$), while the transverse rf field couples to the mode with

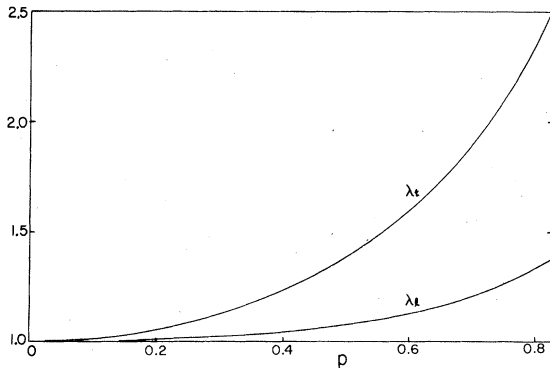


FIG. 5. λ_l and λ_t for $\vec{v}_s \parallel \vec{H}$ (which appear in the NMR frequencies) at the phase boundary are shown as functions of p .

$q = \mp k$, which is easily seen from the expression of the magnetization (15) for a helical texture

$$\begin{aligned} \omega_1 &= \sin\theta \cos(kz) \gamma_t - \sin(kz) g_t, \\ \omega_2 &= \sin\theta \sin(kz) \gamma_t + \cos(kz) g_t, \\ \omega_3 &= f_t + \cos\theta \gamma_t. \end{aligned}$$

Therefore at the phase boundary there appear two longitudinal resonances with

$$\omega_{l1,2} = (\lambda_l \Omega_A^2 + \frac{1}{4}\omega_0^2)^{1/2} \pm \frac{1}{2}\omega_0 \quad (25)$$

and four transverse resonances

$$\begin{aligned} \omega_{t1}^+ &= (\lambda_l \Omega_A^2 + \frac{1}{4}\omega_0^2)^{1/2} + \frac{1}{2}\omega_0, \\ \omega_{t2}^+ &= (\Omega_A^2 + \frac{1}{4}\omega_0^2)^{1/2} - \frac{1}{2}\omega_0, \\ \omega_{t1}^- &= (\Omega_A^2 + \frac{1}{4}\omega_0^2)^{1/2} + \frac{1}{2}\omega_0, \\ \omega_{t2}^- &= (\lambda_l \Omega_A^2 + \frac{1}{4}\omega_0^2)^{1/2} - \frac{1}{2}\omega_0, \end{aligned} \quad (26)$$

where $\lambda_l = \lambda_l + 3k^2$ and the superscripts + and - indicate that the mode couples to M^+ and M^- respectively. Here we have made use of an approximate relation

$$\lambda_l \cong 1 + k^2 \quad (27)$$

at the phase boundary. λ_l at the phase boundary is also shown in Fig. 5 as a function of p . The appearance of four resonance modes in the transverse resonance may be surprising at first glance. However, this is because the helical texture breaks the chiral symmetry along the z direction; M^+ and M^- have different resonance frequencies. The intensities of the longitudinal mode depend linearly on the resonance frequencies and are proportional to $\sin^2\theta$, while the intensities of the transverse mode are proportional to the square of the resonance frequencies as in the case of the parallel texture. If the longitudinal resonance experiment is done in the present configuration, where the external magnetic field is slowly increased, the entrance into the helical regime is signaled by the appearance of the resonance frequencies ω_{l1} and ω_{l2} , whose intensities increase linearly with $h - h_1$ for $h > h_1$. Alternatively the transverse resonance monitors a sudden appearance of four resonances at ω_{t1}^\pm and ω_{t2}^\pm upon entrance into the helical texture. Therefore in spite of obvious difficulties in carrying out NMR experiments in such a small magnetic field ($H \sim 2.30$ Oe), the NMR will provide unique means to detect the existence of the helical texture.

B. $\vec{H} \perp \vec{v}_s$

In this case the uniform texture $\hat{l} \parallel \hat{d} \parallel \vec{v}_s$ gives rise to the usual bulk resonance with $\omega_l = \Omega_A$ and $\omega_t = (\omega_0^2 + \Omega_A^2)^{1/2}$. In order to handle the magnetic

resonance in the helical texture, it is more convenient to introduce new coordinates where the static magnetic field is in the z direction. The new coordinates are obtained by rotating the old ones around the x axis by $-\frac{1}{2}\pi$. Thus the static \hat{d} configuration in the new coordinates is given by

$$\hat{d} = (\sin\theta \cos\phi, -\cos\theta, \sin\theta \sin\phi).$$

To identify the Euler angles with θ and ϕ , we consider the \hat{d} vector to be obtained from $\hat{d} \parallel \hat{y}$ by the rotation $R(\alpha, \beta, \gamma)$,

$$\begin{aligned} \hat{d} = & -(\sin\alpha \cos\gamma + \cos\alpha \cos\beta \sin\gamma)\hat{x} \\ & + (\cos\alpha \cos\gamma - \sin\alpha \cos\beta \sin\gamma)\hat{y} \\ & + \sin\beta \sin\gamma \hat{z}. \end{aligned} \quad (28)$$

Comparing Eq. (28) with \hat{d} above, we obtain

$$\alpha = \pi, \quad \beta = \phi, \quad \text{and} \quad \gamma = \theta.$$

The spin fluctuation around the helical texture is then handled by assuming

$$\beta = \phi + f \quad \text{and} \quad \gamma = \theta + g,$$

where f and g are small fluctuations. The linearized equations for α , f , and g are given by

$$\begin{aligned} \alpha_u + \cos\phi g_u &= 0, \\ f_u - \omega_0 \sin\phi g_t &= -\frac{1}{2} \Omega_A^2 \frac{\delta G}{\delta f}, \end{aligned} \quad (29)$$

$$g_u + \cos\phi \alpha_u + \omega_0 \sin\phi f_t = -\frac{1}{2} \Omega_A^2 \frac{\delta G}{\delta g},$$

where

$$\begin{aligned} \frac{1}{2} \frac{\delta G}{\delta f} &= -\sin^2\theta(1+s)f_{yy} + \cos(\theta-\chi) \sin\chi \sin\theta f \\ &\quad - (1+s) \sin(2\theta) \phi_y g_y, \\ \frac{1}{2} \frac{\delta G}{\delta g} &= (1+s)(-g_{yy} + \{\cos(2\theta) \phi_y^2 + \cos[2(\theta-\chi)]\}g \\ &\quad + \sin(2\theta) \phi_y f_y). \end{aligned} \quad (30)$$

Here we are in the new coordinates, where the axis of the helical texture is in the y direction. First of all we can eliminate α from Eq. (29). Furthermore in the vicinity of the phase boundary where both θ and χ are small, $\delta G/\delta f$ is completely negligible. Then we can eliminate f from Eq. (29) as well. The resonance frequencies ω are determined by the eigenvalue equation;

$$\sin^2\phi(\omega^2 - \omega_0^2)g = \Omega_A^2[-g_{yy} + (1 + \phi_y^2)g]. \quad (31)$$

Since ϕ depends on y as $\tan\phi = (v'/u') \tan(ky)$, Eq. (31) may be approximated by a Mathieu equation

$$g_{yy} + [a - 2q \cos(2ky)]g = 0, \quad (32)$$

with

$$\begin{aligned} a &= \frac{(X)^{1/2}}{[1 + (X)^{1/2}]} \left[\frac{\omega^2 - \omega_0^2}{\Omega_A^2} \right] - \left[1 + \frac{k^2}{2(X)^{1/2}}(1+X) \right], \\ 2q &= \frac{2(X)^{1/2}}{[1 + (X)^{1/2}]^2} \left[\frac{\omega^2 - \omega_0^2}{\Omega_A^2} \right] - \frac{k^2}{(X)^{1/2}}(1-X), \end{aligned} \quad (33)$$

and

$$X = (v'/u')^2.$$

Here we have expanded $\sin^2\phi$ and ϕ_y^2 in a Fourier series retaining only the first two terms. The above approximation should be excellent when $X \sim 1$. As the field h increases, X rapidly decreases from unity and at $h=1$, we have $X \approx 0.41$. Therefore we believe that the above approximation is valid only for $h < 1$.

From the expression of the magnetization (15), we note also that the longitudinal rf field couples dominantly to the Mathieu function¹⁶ ce_1 (there is a weak

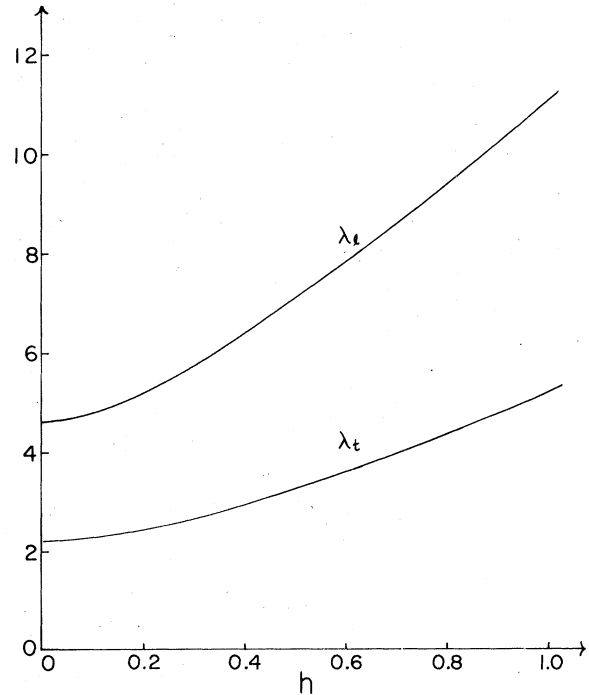


FIG. 6. λ_r and λ_t for $\vec{v}_s \perp \vec{H}$ at the phase boundary are shown.

coupling to ce_3 , etc.), while the transverse rf field couples to se_1 . The resonance frequencies are then given by

$$\omega_l^2 = \omega_0^2 + \lambda_l \Omega_A^2$$

and

$$\omega_t^2 = \omega_0^2 + \lambda_t \Omega_A^2$$

for the longitudinal and the transverse resonance, where λ_l and λ_t are determined numerically along the phase boundary. These results are shown as functions of h in Fig. 6. We limit our analysis to the region $0 < h < 1$, since as already mentioned, for larger h , the Mathieu equation (32) no longer is a good approximation. Again the appearance of the helical texture is signaled by sudden jumps of NMR frequencies for both the longitudinal and transverse resonance.

In the present geometry we recover the Pythagorean relation, although ω_l^2 contains the ω_0^2 term in contrast to the usual bulk case.

IV. CONCLUDING REMARKS

Limiting ourselves to two particular geometries in the Ginzburg-Landau regime, we have shown that the uniform texture with $(\hat{l} \parallel \hat{d} \parallel \vec{v}_s)$ in $^3\text{He-A}$ transforms into a helical texture in the presence of magnetic fields via a second-order transition. Making use of the Ginzburg-Landau approach, we have determined the phase diagrams and the \hat{l} and \hat{d} configurations of the helical textures in the vicinity of the phase boundary. We have shown that the helical texture possesses anomalous magnetic resonances, which shall provide an unambiguous signature of the helical texture. The sound attenuation with wave vector \vec{q} with a finite angle to \vec{v}_s may exhibit a jump when $q_z = 2k$ with k the wave number of helical texture just like in a cholesteric liquid.^{17,18} This possibility is currently examined.

When the superflow is induced by heat current, it is very likely that the whole texture moves uniformly with \vec{v}_n , the normal flow. In such a situation the heat flow produces a periodic variation in the \hat{l} field with a period $\tau (\equiv 1/v_n k)$. When the heat flow is kept constant, τ varies like $(1 - T/T_c)^{-1}$ since $k \sim v_s$. This may account for the periodic orbital motion observed by Paulson, Krusius, and Wheatley.¹⁹

ACKNOWLEDGMENT

We thank Robert Kleinberg for stimulating discussions on his experimental data and Robijn Bruinsma for suggesting a possibility of detecting the helical pitch by sound attenuation. This work is supported by the NSF under Grant No. DMR76-21032.

APPENDIX A: HELICAL TEXTURES IN A TILTED MAGNETIC FIELD

We study here the effect of a small misalignment between the magnetic field and the superflow on the p - h diagram. Without loss of generality we can assume that \vec{v}_s is along the z direction, and

$$\vec{h} = h(0, \sin\eta, \cos\eta) . \quad (\text{A1})$$

The free-energy G is given by Eq. (1) except that the magnetic field energy has to be replaced by

$$h^2(\sin\eta \sin\theta \sin\phi + \cos\eta \cos\theta)^2 .$$

In terms of u, v, u' , and v' , G can be written

$$G = G_0 + G_1' + G_2' + \dots , \quad (\text{A2})$$

where G_1' is again given by Eq. (3) except the term $-h^2(u'^2 + v'^2)$ is replaced by

$$h^2(\sin 2\eta v' - \cos^2 \eta u'^2 - \cos 2\eta v'^2)$$

and G_2' by

$$G_2' = G_2 - \frac{1}{2} h^2 \sin 2\eta v' (u'^2 + v'^2) . \quad (\text{A3})$$

Now G contains the linear and the third-order terms in u' and v' due to nonzero η . Therefore the uniform state with $\hat{l} \parallel \hat{d} \parallel \hat{z}$ is no longer stationary. In order to find the stationary uniform state for given p and h , we first minimize G with respect to small shifts in u, v, u' , and v' . To the leading order in η , the stationary uniform state is given by

$$\begin{aligned} u &= u' = 0 , \\ v &= \bar{v} \left[\equiv -\frac{1}{2} h^2 \sin 2\eta [p^2 - h^2 \cos 2\eta (1 + p^2)]^{-1} \right] , \quad (\text{A4}) \\ v' &= \bar{v}' \left[\equiv (1 + p^2) \bar{v} \right] . \end{aligned}$$

Furthermore we can study the helical instability of the uniform texture by writing

$$u = u_0 \cos kz , \quad v = \bar{v} + v_0 \sin kz , \quad (\text{A5})$$

$$u' = u_0' \cos kz , \quad v' = \bar{v}' + v_0' \sin kz .$$

Substituting these in Eq. (A2) and taking the space average, and then eliminating u' and v' by minimizing the quadratic terms in u_0' and v_0' , we obtain

$$\langle G \rangle = \langle G_0 \rangle + A(k) \bar{u}_0^2 + \dots , \quad (\text{A6})$$

where

$$\begin{aligned}
\tilde{u}_0 &= (u_0 v_0)^{1/2} , \\
A(k) &= K_1 K_2 - (3 - \frac{11}{2} \bar{v}^2) p k , \\
K_1 &= [1 + p^2 + \frac{3}{2} k^2 - \bar{v}^2 [2k^2 + (3 + p^2) p^2] - a]^{1/2} , \\
K_2 &= [1 + p^2 + \frac{3}{2} k^2 - \bar{v}^2 [1 + \frac{1}{2} k^2 - (7 + 2p^2) p^2] - b]^{1/2} , \\
a &= (1 - \frac{1}{2} p^4 \bar{v}^2)^2 [1 + k^2 - h^2 \cos^2 \eta + \bar{v}^2 (k^2 + p^2) - \frac{1}{2} \sin(2\eta) \bar{v} (1 + p^2) h^2]^{-1} , \\
b &= [1 + (1 + p^2 - \frac{3}{2} p^4) \bar{v}^2]^2 [1 + k^2 - h^2 \cos 2\eta + \bar{v}^2 [2k^2 (1 + p^2 + \frac{1}{2} p^4) + 1 + 3p^2] - \frac{3}{2} \sin(2\eta) \bar{v} (1 + p^2) h^2]^{-1} .
\end{aligned} \tag{A7}$$

Then the phase boundary between the uniform texture and the helical texture is determined by the conditions

$$\frac{\partial A}{\partial k} = 0 \text{ and } A = 0 . \tag{A8}$$

The actual construction of the phase diagram is quite straightforward though tedious. We shall now give the results in the limiting cases. Near the origin the phase boundary is given by

$$p = (10)^{1/2} h (1 - \frac{338}{405} \eta^2) \text{ for small } \eta , \tag{A9}$$

while in the limit $h \rightarrow 0$

$$p_c = p_{c0} [1 - 2.10 h^2 (\cos^2 \eta + \cos 2\eta)] , \tag{A10}$$

where $p_{c0} = 0.826$ is the limiting p value for $\eta = 0$.

APPENDIX B: STABILITY OF THE PARALLEL TEXTURE

Here we analyze the stability of the parallel texture ($\hat{l} \parallel \hat{d} \parallel \bar{\nabla}_s$) against general fluctuations of \hat{d} and \hat{l} . We find that the initial instability is triggered by a purely longitudinal fluctuation as assumed in the text. Following the BHM analysis,⁵ but assuming that \hat{l} and \hat{d} are no longer necessarily parallel to each other, the total free-energy F of $^3\text{He-A}$ is given by

$$F = F_{\text{kin}} + F_D + F_H ,$$

where

$$\begin{aligned}
F_{\text{kin}} &= \int d^3 r [\frac{1}{2} \rho_s v_s^2 - \frac{1}{2} \rho_0 (\hat{l} \cdot \bar{\nabla}_s)^2 + c (\bar{\nabla}_s \cdot \bar{\nabla} \times \hat{l}) - c_0 (\bar{\nabla}_s \cdot \hat{l}) (\hat{l} \cdot \bar{\nabla} \times \hat{l}) + \frac{1}{2} K_s (\bar{\nabla} \cdot \hat{l})^2 + \frac{1}{2} K_t (\hat{l} \cdot \bar{\nabla} \times \hat{l})^2 \\
&\quad + \frac{1}{2} K_b (\hat{l} \times (\bar{\nabla} \times \hat{l}))^2 + \frac{1}{2} \rho_s^{\text{spin}} | \bar{\nabla} \cdot \hat{d} |^2 - \frac{1}{2} \rho_0^{\text{spin}} (\hat{l} \cdot \bar{\nabla}) \hat{d}^2] , \\
F_D &= - \frac{1}{2} \chi_N \Omega_A^2 \int d^3 r (\hat{l} \cdot \hat{d})^2 , \\
F_H &= \frac{1}{2} (\Delta \chi) \gamma_0^2 \int d^3 r (\bar{\mathbf{H}} \cdot \hat{d})^2 ,
\end{aligned} \tag{B1}$$

where K_s , K_t , etc, here denote the contributions from the orbital component only, F_D is the dipole energy and F_H is the magnetic anisotropy energy. In particular in the Ginzburg-Landau regime we have

$$\begin{aligned}
\rho_0 &= c_0 = \frac{1}{2} \rho_s = \frac{1}{2} \rho_s^{\text{spin}} = \rho_0^{\text{spin}} , \\
3K_s &= 3K_t = K_b = \frac{3}{4} \rho_s .
\end{aligned} \tag{B2}$$

Furthermore in reduced units, we can set

$$\chi_N \Omega_A^2 = (\Delta \chi) \omega_0^2 = \rho_s . \tag{B3}$$

The small fluctuations of \hat{l} and \hat{d} can be written

$$\begin{aligned}
\delta \hat{l} &= \bar{\Gamma}' - \frac{1}{2} l'^2 \hat{z} , \\
\delta \hat{d} &= \bar{\mathbf{d}}' - \frac{1}{2} d'^2 \hat{z} ,
\end{aligned} \tag{B4}$$

where $\bar{\Gamma}' = (u, v, 0)$ and $\bar{\mathbf{d}}' = (u', v', 0)$. Similarly

$$\bar{\nabla}_s = p \hat{z} + \bar{\nabla} \phi + \frac{1}{2} (u \bar{\nabla} v - v \bar{\nabla} u) . \tag{B5}$$

Substituting Eqs. (B4) and (B5) into Eq. (B1), we can expand the free-energy in powers of small fluctuations. Assuming that fluctuations are characterized by a wave vector $\bar{\mathbf{k}} = (q_x, q_y, k)$, we can eliminate $\phi(\bar{\mathbf{k}})$, $u'(\bar{\mathbf{k}})$, and $v'(\bar{\mathbf{k}})$ by minimizing the quadratic

term in $\phi u'$, and v' and we obtain

$$F = F_0 + \sum_{\vec{k}} \left[\frac{1}{2} K_s |\vec{q} \cdot \vec{\Gamma}'|^2 + \frac{1}{2} K_t |\vec{q} \times \vec{\Gamma}'|^2 + \frac{1}{2} K_b k^2 |\vec{\Gamma}'|^2 + \left(\frac{1}{2} \rho_0 p^2 + \lambda_D [1 - \lambda_D (\lambda_D - \lambda_H H^2 + \frac{1}{2} \rho_s^{\text{spin}} q^2 + \frac{1}{2} \rho_0^{\text{spin}} k^2)^{-1}] \right) |\vec{\Gamma}'|^2 \right. \\ \left. + \left(\frac{1}{2} \rho_{s11} + c_0 \right) p \vec{k} \cdot \text{Im}(\vec{\Gamma}'^* \times \vec{\Gamma}') - \frac{1}{2(\rho_s q^2 + \rho_{s11} k^2)} [c_0 k^2 |\vec{q} \times \vec{\Gamma}'|^2 + \rho_0 (\vec{q} \cdot \vec{\Gamma}')^2 p^2 + \rho_{s11} c_0 p q^2 \vec{k} \cdot \text{Im}(\vec{\Gamma}'^* \times \vec{\Gamma}')] \right] + O(\vec{\Gamma}'^4) \quad (\text{B6})$$

and

$$\vec{d}'(\vec{k}) = \lambda_D (\lambda_D - \lambda_H H^2 + \frac{1}{2} \rho_s^{\text{spin}} q^2 + \frac{1}{2} \rho_0^{\text{spin}} k^2)^{-1} \vec{\Gamma}'(\vec{k}) \quad (\text{B7})$$

where

$$\rho_{s11} = \rho_s - \rho_0, \quad \lambda_D = \chi_N \Omega_A^2,$$

and

$$\lambda_H = (\Delta \chi) \gamma_0^2.$$

Here we have assumed that $\vec{H} \parallel \vec{v}_s$.

We can further simplify the free energy (B6), by assuming that

$$u = u_0 e^{i\vec{q} \cdot \vec{r}} \cos(kz), \quad v = v_0 e^{i\vec{q} \cdot \vec{r}} \sin(kz),$$

as

$$F = F_0 + \frac{1}{2} \lambda_D A(\vec{k}) \vec{u}_0^2 + O(\vec{u}_0^4), \quad (\text{B8}) \\ A(\vec{k}) = K_1 K_2 - K_{12}^2,$$

where

$$\vec{u}_0^2 = u_0 v_0, \quad (v_0/u_0) = K_1/K_2. \quad (\text{B9})$$

In the Ginzburg-Landau regime K_1 , K_2 , and $K_{1,2}$ are given by

$$K_1^2 = 1 + [1 - q^2(k^2 + 2q^2)^{-1}] p^2 \\ + \frac{1}{2} (3k^2 + q^2) - (1 + k^2 + 2q^2 - h^2)^{-1}, \\ K_2^2 = 1 + p^2 + \frac{1}{2} [3 - 4q^2(k^2 + 2q^2)^{-1}] k^2 \\ - (1 + k^2 + 2q^2 - h^2)^{-1},$$

and

$$K_{12}^2 = [3 - q^2(k^2 + 2q^2)^{-1}] p k. \quad (\text{B10})$$

where we have written K_1 , K_2 , and K_{12} in reduced units.

Now the phase boundary, where the uniform texture becomes unstable, is given by

$$\frac{\partial A}{\partial k} = 0 \quad \text{and} \quad A = 0. \quad (\text{B11})$$

For small q (i.e., $q^2 \ll k^2$), it is shown analytically that

$$A(q, k) > A(0, k).$$

More generally a numerical analysis shows that the longitudinal fluctuation is responsible for the instability of uniform texture.

In the perpendicular geometry ($\vec{H} \perp \vec{v}_s$), a similar analysis was carried out, although it is much more involved and we will not reproduce it here. We find again that the longitudinal instability precedes other instabilities.

¹G. E. Volovik and V. P. Mineyev (unpublished); see also N. D. Mermin, in *Quantum Liquid*, edited by J. Ruvalds and T. Regge (North-Holland, Amsterdam, 1978).

²N. D. Mermin and T. L. Ho, Phys. Rev. Lett. **36**, 594 (1976).

³P. W. Anderson and G. Toulouse, Phys. Rev. Lett. **38**, 508 (1977).

⁴T. L. Ho, Phys. Rev. B **18**, 1144 (1978).

⁵P. Bhattacharyya, T. L. Ho, and N. D. Mermin, Phys. Rev. Lett. **39**, 1290 (1977); M. C. Cross and M. Liu, J. Phys. C **11**, 1795 (1978).

⁶M. C. Cross, J. Low Temp. Phys. **21**, 525 (1975).

⁷A. L. Fetter, Phys. Rev. Lett. **40**, 1656 (1978).

⁸H. Kleinert, Y. R. Lin-Liu, and K. Maki, J. Phys. (Paris) **39**, C6-59 (1978); and Phys. Lett. A **70**, 27 (1979).

⁹Y. R. Lin-Liu, K. Maki, and D. Vollhardt, J. Phys. Lett. (Paris) **39**, L-381 (1978).

¹⁰S. Takagi, Prog. Theor. Phys. **60**, 934 (1978); W. N. Saslow and C. R. Hu, J. Phys. Lett. (Paris) **39**, L-379 (1978); J. Hook and H. E. Hall (unpublished).

¹¹A. J. Leggett, Ann. Phys. (N.Y.) **85**, 11 (1974).

¹²R. Kleinberg, Phys. Rev. Lett. **42**, 182 (1978); J. Low

Temp. Phys. (to be published).

¹³We have slightly modified notations as well as units from those given in Ref. 9.

¹⁴This disagrees with an earlier result by Fetter [A. L. Fetter, Phys. Lett. A **54**, 63 (1975)], except in the limit $\omega_0 \gg \Omega_A$, where his result is valid.

¹⁵K. Maki, Phys. Rev. B **11**, 4264 (1975). Although the spin Lagrangian in this reference is derived for ³He-B, the corresponding Lagrangian for ³He-A is easily obtained from Eq. (12) by identifying $\chi_{ij} = \chi_N \delta_{ij}$,

$$(\chi^j)_{ij}^{lm} = [\rho_s^{\text{spin}} (\delta_{lm} - \hat{l}_i \hat{l}_m) + \rho_s^{\text{spin}} \hat{l}_i^m] (\delta_{ij} - \hat{a}_i \hat{a}_j).$$

¹⁶M. Abramowitz and I. A. Stegun, *Handbook of Mathematical Functions* (Dover, New York, 1970).

¹⁷J. D. Parsons and Charles F. Hayes, Solid State Commun. **15**, 429 (1974).

¹⁸I. Muscatariu, S. Bhattacharya, and J. B. Ketterson, Phys. Rev. Lett. **35**, 1584 (1975).

¹⁹D. N. Paulson, M. Krusius, and J. C. Wheatley, Phys. Rev. Lett. **37**, 599 (1976).